Quarterly Journal of the Royal Meteorological Society
A journal of the atmospheric sciences and physical oceanography

Development Mechanisms for Mediterranean Tropical-Like Cyclones (Medicanes)

Journal:	*QJRMS*
Manuscript ID	Draft
Wiley - Manuscript type:	Research Article
Date Submitted by the Author:	n/a
Complete List of Authors:	Miglietta, Mario; ISAC-CNR Rotunno, Richard; NCAR, ;
Keywords:	Medicanes, tropical-like cyclones, potential vorticity, Mesoscale < 2. Scale, Convection < 3. Physical phenomenon, Severe weather < 3. Physical phenomenon, sea surface fluxes
Country Keywords:	Italy, Spain, France, Greece, Tunisia

SCHOLARONE™
Manuscripts

Development Mechanisms for Mediterranean tropical-like cyclones (Medicanes)

Mario Marcello Miglietta*

ISAC-CNR, Padua/Lecce, Italy

Richard Rotunno

NCAR, Boulder, USA

For Peer Review

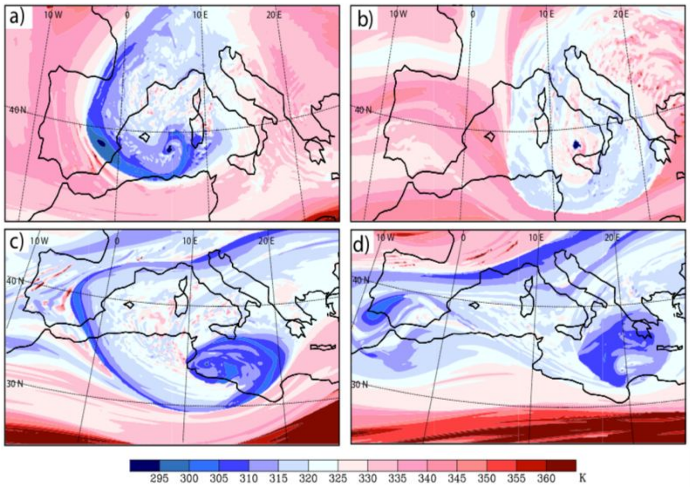

A classification of Medicanes into different categories is proposed. The first category includes cyclones dominated in their mature stage by air-sea interaction, where the latter enables the vortex to sustain itself: an isolated minimum of θ (color, K) on the 2 PVU surface is diabatically generated by convection (panel b), is not connected with any large-scale feature as in the early stages (panel a). The second category includes cyclones in which both air-sea interaction and baroclinic processes are important, and the vortex remains connected with the large-scale PV structure in which it formed (panel c) even in its mature stage (panel d).

For Peer Review

Development Mechanisms for Mediterranean Tropical-Like Cyclones (Medicanes)

Mario Marcello Miglietta*

ISAC-CNR, Padua/Lecce, Italy

Richard Rotunno

NCAR°, Boulder, USA

°The National Center for Atmospheric Research is sponsored by the National Science Foundation.

* *Corresponding author address:* Mario Marcello Miglietta, CNR-ISAC, corso Stati Uniti 4, 35127 Padua, Italy.
E-mail: m.miglietta@isac.cnr.it

For Peer Review

Keywords: Medicanes; tropical-like cyclones; potential vorticity; mesoscale; convection; severe weather; sea surface fluxes

ABSTRACT

Midlatitude cyclones with characteristics similar to tropical cyclones (also known as Tropical-Like Cyclones, TLCs, or Medicanes) are sometimes observed in the Mediterranean region. The Wind Induced Surface Heat Exchange (WISHE) mechanism has been considered responsible for their development, in analogy with tropical-cyclone theory. However, some recent papers have proposed a different explanation, suggesting that the deep warm core in the TLC is mainly an effect of the seclusion of warm air in the cyclone core. To investigate the latter hypothesis, two case studies of Mediterranean TLCs are analyzed here by means of high-resolution numerical experiments. The evolution of the near-surface equivalent potential temperature is followed along back-trajectories around the cyclone center, showing for both cases a strong heating when the parcel moves from the outer part of the cyclone to its inner, warmer core. Sensitivity experiments clarify the mechanism of cyclone intensification and the way the warm-core structure is generated, showing that sea-surface fluxes and/or condensation latent heating are fundamental to explain the intensification of the cyclones. However, the importance of air-sea interaction processes is case dependent. For the first cyclone, the intense sea surface fluxes, associated with Tramontane and Cierzo winds over the western Mediterranean Sea, transfer a large amount of energy from the ocean to the atmosphere in the area where the cyclone developed, so that the vortex is able sustain itself in a barotropic environment and reach a tropical-like structure at a later stage in its lifetime. For the second cyclone, the cyclone never develops a fully tropical-like structure, evolving in the baroclinic environment associated with the potential vorticity streamer in which the cyclone formed. Based on the distinction emerging in this and other papers, a classification of Medicanes in three different categories is proposed.

For Peer Review

1. Introduction

In the last few years, a renewed interest has emerged in the analysis of Mediterranean vortices with characteristics similar to tropical cyclones. Such vortices, better known as Tropical-Like Cyclones (TLCs) or MEDIterranean hurriCANES (Medicanes), show a remarkable similarity to their tropical counterparts both for their appearance in satellite images and for their dynamical and thermodynamic features. In fact, they are characterized by the presence of an "eye" of mostly calm weather, a warm-core anomaly that is maximum near the surface, weak vertical wind shear, a strong rotation around the pressure minimum, an eyewall with convective cells, from which rainbands extend, induced sea level rise and storm surge.

However, in contrast with tropical cyclones, their lifetime is restricted to a few days, due to the limited extent of the Mediterranean Sea, which is their main source of energy; also, they attain fully tropical characteristics only for a short period, while extratropical features prevail for most of their lifetime (Miglietta et al., 2011, 2013); the horizontal extent is generally confined to a few hundred km; the intensity rarely exceeds category 1 of hurricane strength. Since they form at mid-latitudes, where baroclinicity is generally large, environmental conditions of weak vertical wind shear, necessary for their development, are unusual, limiting the number of occurrences to 1-2 events per year (Cavicchia et al., 2014). The sea surface temperatures (SST) over which they form are below the threshold of 26.5 °C observed for most tropical cyclones, since cold-air intrusions in the extra-tropics may increase the conversion efficiency of thermal energy into mechanical energy (Palmén, 1956), making possible the development of a TLC even in January. This mechanism is similar to that responsible for the formation of tropical cyclones farther from the Equator, close to the Tropics (Mc Taggart-Cowen et al., 2015).

After the paper by Hart (2003), there has been an increasing awareness that a continuum of cyclones exists between tropical and extratropical systems, among which there is no clear-cut separation. As

For Peer Review

discussed in Garde et al. (2010), there is a growing interest to objectively quantify the gray areas between the two categories and to better explore the processes responsible for the transition between them. Within this perspective, Gaertner et al. (2017) have considered Mediterranean TLC as part of the wider category of subtropical cyclones, which have been observed in several basins of the world, such as the Atlantic Ocean (González-Alemán et al. 2015; Yanase and Niino, 2018), the Pacific Ocean (Garde et al., 2010), and the Australian west coast (Cavicchia et al., 2018). Their peculiarity is the fact they form as baroclinic, extra-tropical cyclones, eventually evolving into tropical systems (as much of their energy comes from convective clouds).

Rasmussen and Zick (1987) pointed out the similarity of TLCs with polar lows. Businger and Reed (1989) considered the Mediterranean TLC as a particular case of polar lows, cyclones forming in cold polar or arctic air advected over relatively warmer waters, for example in northern Europe (Nordeng, 1990) and in the Japan Sea (Watanabe and Niino, 2014). However, Reale and Atlas (2001) noted that in TLCs latent heat fluxes are much stronger than sensible heat, while sensible and latent heat are normally of comparable magnitude in polar lows. Also, barotropic instability seems to contribute to TLC development, while it is not a cause for the development of polar lows.

For Peer Review

All these categories of hybrid cyclones share with tropical cyclones the mechanism of development in the "tropical-like" part of their lifetime, the so-called Wind Induced Surface Heat Exchange (WISHE; Emanuel, 1986; Rotunno and Emanuel, 1987): these storms are developed and maintained against dissipation entirely by self-induced sea surface fluxes with virtually no contribution from preexisting CAPE, so they result from an air-sea interaction instability. The role of vertical motion is to redistribute the heat acquired from sea surface to keep the environment close to moist neutrality (Emanuel and Rotunno, 1989).

The relevance of this mechanism for Mediterranean TLC has been successfully tested in several case studies (e.g., Emanuel, 2005; Moscatello et al., 2008a). However, some recent papers have proposed that the seclusion by colder air occurring in the extratropical part of their lifetime contributes to the generation of a warm core extending also in the upper troposphere. "The tropical transition would take place as the cyclones undergo a warm seclusion, … the upper-tropospheric warm core is also a result of the warm seclusion" (Mazza et al., 2017). Even if the authors do not disregard the role of surface fluxes in the tropical transition, they conclude that "the analysis of the simulations does not provide sufficient evidence to sustain that a cooperative process similar to WISHE is in place". Similarly, Fita and Flounas (2018) state for another Mediterranean TLC that "despite its importance, it would be delicate to suggest that diabatic heating due to convection is able to sustain the medicane vortex similarly to the WISHE mechanism. In fact, the high positive potential vorticity (PV) anomalies within the upper troposphere could play a critical role in the development of the surface cyclone … it is deep convection triggered by the PV streamer that tends to provide low level heating and it is warm air seclusion that makes the system to attain a warm core with respect to its environment."

The purpose of the present paper is to analyze the mechanisms of development of the cyclones analyzed in the latter two papers in order to identify the role of air-sea interaction in their intensification. The paper is organized as follows. The two case studies are briefly described in Section 2. The setup of the numerical experiments is shown in Section 3, while results are presented in Section 4. Further discussion and conclusions are, respectively, in Sections 5 and 6.

2. Case studies

The two cyclones analyzed here are among the Mediterranean TLCs most investigated in the literature. The first case study is analyzed in detail in Reale and Atlas (2001); these authors were able to follow the evolution of the cyclone with the help of satellite images and large-scale analyses. After a first TLC

For Peer Review

developed between Tunisia and Sicily on 4 October 1996, which was responsible for severe floods in Sicily and in the southern part of Calabria (southern Italy), a new cyclone formed north of the Algerian coast on October 6, beneath an upper-level cold cut-off low which had formed over the western Mediterranean (Reale and Atlas, 2001, Fig. 8). In this earlier phase, the cyclone still showed extratropical features. Subsequently, the cyclone moved northward between Sardinia and the Balearic Islands, as it reduced in size and increased its intensity. The environment was characterized by a strong westerly jet to the south of the storm (Reale and Atlas, 2001, Fig. 20), which played a key role in its development by barotropic instability. The cyclone kept intensifying, showing on October 7 a perfect alignment of the mean sea-level pressure minimum with the 500 hPa cut-off, a warm-core structure, and an eye-like appearance in the satellite images; next, on October 8, the storm moved eastward, marginally crossing southeastern Sardinia and then moving over the Tyrrhenian Sea. On October 9, the cyclone moved southward still over the Tyrrhenian Sea, from the east of Sardinia to the north of Sicily, re-intensifying and becoming smaller in size (Reale and Atlas, 2001, Fig. 11). The strong damage reported over the Aeolian islands and the wind speed of 22.5 m/s recorded in the island of Ustica suggest that the hurricane category 1 level was probably reached in this phase. On October 10 the cyclone made landfall and started dissipating.

The second cyclone is described in Fita and Flounas (2018). On 9 December 2005, an elongated trough extended toward the western Mediterranean from Scandinavia forming an upper-level cut-off. In the following days, the cut-off remained trapped in the western Mediterranean, in between the Azores and the Siberian Highs. At low levels, on 12 December 2005 a weak pressure minimum, rapidly moving northward, appeared over western Libya (Fita and Flounas, 2018, Fig. 2). On December 13, the cyclone was over the Mediterranean Sea, where it rapidly intensified, remaining nearly stationary close to the east coast of Tunisia, and started to show a symmetric deep warm core (Fita and Flounas, 2018, Fig. 5). Next, the Medicane moved eastward, to the north of the Libyan coast, progressively weakening on

For Peer Review

December 14. The eastward movement of the Medicane close to the northern coast of Africa (Libya, Egypt) was characterized by significant dust advection (T. Giannaros, personal communication). The cyclone kept moving eastward on December 15 and progressively weakened while the upper-level cut-off was absorbed by the main zonal circulation, appearing as the extreme tip of the trough extending southward from Russia. With a weaker intensity, the cyclone made landfall on December 16 at the Turkish coast of the Mediterranean, to the southeast of Cyprus (Fita and Flounas, 2018, Fig. 2).

3. Numerical setup

The present numerical simulations were performed with the Advanced Research Weather Research and Forecasting (WRF-ARW) model, version 4.0 (www.wrf-model.org; Skamarock et al., 2008), in order to simulate the two Mediterranean TLCs discussed in Section 2. WRF is a numerical weather prediction system that solves the fully compressible, nonhydrostatic Euler equations, using, in the latest versions, hybrid vertical coordinates that are terrain-following near the surface and become isobaric at higher levels. Forty vertical levels are used in the present simulations, more closely spaced in the PBL. Simulations are performed on two two-way nested domains, respectively of 9 and 3 km grid spacing: the external domain extends over 400/480 (first/second case in east–west direction) and 300/280 (in north–south direction) grid points, the inner domain over 625 and 403 grid points in both cases. The high-resolution of the inner grid allows explicit convection at the system scale, which is important to properly reproduce the cyclone evolution (Cioni et al., 2018, p. 1609). The grid set-up is different between the two experiments in order to cover the tracks for the whole lifetime of the respective cyclones.

Large-scale initial/boundary conditions are provided by the 6-hourly ERA-INTERIM reanalysis fields, whose resolution is approximately 80 km (T255 spectral resolution). Different starting times and convection-parameterization schemes have been tested to initialize the model simulations. Although the differences in track among the different implementations are generally limited to few km, such a small

For Peer Review

shift may however change the cyclone location from sea to land and dramatically affect the sea-surface fluxes and the following evolution. The best (control) simulations for the two cases start, respectively, at 0000 UTC, 4 October 1996 and last for 144 hours, and at 0000, 12 December 2005, and last for 96 hours.

For the first case, the control run is implemented with: Thompson et al. (2008) microphysics, Rapid Radiative Transfer Model for longwave radiation (Mlawer et al., 1997), Dudhia (1998) shortwave radiation, Unified Noah land-surface model (Niu et al., 2011), Mellor-Yamada-Janjic TKE scheme (Janjic, 2001) scheme; the Betts and Miller (1993) convection scheme is activated on the coarser grid, which emerged as the best in terms of track, as in Miglietta et al. (2015). For the second case study, the implementation follows that of Fita and Flounas (2018): the WRF Single Model-5 class microphysics (Hong et al., 2004), the five-layer thermal-diffusion scheme for land-surface processes (Dudhia, 1996), the Yonsei University planetary-boundary-layer scheme (Hong et al., 2006). As in Fita and Flounas (2018), the Kain-Fritsch (Kain, 2004) convection scheme is employed, since it provides a more realistic track compared to the simulation using the Betts-Miller scheme for this case (which produces an erroneous landfall over northern Libya). Convection is treated explicitly on the inner grid in both experiments. Output fields are saved every hour.

For Peer Review

Sensitivity experiments are performed to investigate the role of sea-surface fluxes and latent-heat release associated with convection. These additional simulations (respectively, without condensational latent heat -No latent heat-, without sea surface fluxes -No fluxes-, or without both -No all-) are restart runs, with the initial fields provided by the control simulations (with full physics) respectively at 1800 UTC, 6 October and at 1800 UTC, 13 December, some hours before the cyclones reached their maximum intensity in the early stages of their lifetime. The absence of latent-heat release and/or surface fluxes in these sensitivity experiments allow one to distinguish the role of baroclinic instability in the absence of air-sea interaction and convective processes.

4. Results

Numerical simulations are discussed here to examine the relevance of air-sea-interaction processes in the development of these two tropical-like cyclones.

a) October 1996 case

The WRF model simulation is able to simulate relatively accurately the observed track of the cyclone, as derived from satellite images. Figure 1 shows the simulated track; apart from being slightly shifted to the south compared to infrared and visible Meteosat satellite images (Reale and Atlas, 2001; Mazza et al., 2017) near Sardinia, the model reproduces the cyclone evolution well. The simulated and the observed cyclone positions (eye-based location taken from satellite images) are shown at 1000 UTC, Oct 7 (red asterisk), at 1500 UTC, Oct 8 (green "o"), at 1030 UTC, Oct 9 (blue "x").

The first part of the trajectory, to the west of Sardinia, is reproduced accurately; later, during its eastward displacement, the cyclone remains slightly to the south of the observations, so that it does not make landfall over Sardinia, as observed, possibly making the simulated cyclone susceptible to a more intense deepening compared to observations (the sea surface fluxes have a longer period to affect the cyclone). The model recovers the right cyclone location over the Tyrrhenian Sea, where the cyclone reintensifies in agreement with the observations (Reale and Atlas, 2001), while the landfall over Sicily is displaced to the west with respect to the observed landfall which was between Sicily and Calabria.

In order to analyze how the air-sea interaction affects the development of the cyclone, the 900 hPa equivalent potential temperature θ_e and wind vectors are shown when the cyclone is still west of Sardinia (2100 UTC, 7 October 1996), in the control run (Fig. 2a) and in the sensitivity experiment without

For Peer Review

enthalpy fluxes (No-fluxes run; Fig. 2b). Results show a maximum of $\theta_e$in the control run near the cyclone, which is identified by the center of the cyclonic circulation at the same pressure level. The maximum is surrounded by lower values of $\theta_e$both on the eastern side of the cyclone and on its western side, associated with cold-air advection, which secludes the cyclone warm core.

It might be argued that the high temperature and water vapor content near the low pressure are the result of horizontal advection, as in a purely baroclinic disturbance. In order to test this hypothesis, the evolution of θ_e is analyzed for a parcel whose Lagrangian back-trajectory ends at 2100 UTC, 7 October 1996, representative of the trajectories ending in the southern part of the warm core of the cyclone at low levels (900 hPa). This low-level air parcel moves along an inward spiraling convective band, from the outskirts toward the eye. Figure 3 shows an increase in θ_e during the experiment, in particular during the last 4 h (track shown in Fig. 2a), when the parcel remains at a relatively constant height, while its θ_e increases by almost 10 K. This increase occurs when the parcel moves to the area affected by the largest sea surface fluxes (see Section 5) and intense convection. In contrast, the θ_e of the parcel does not change appreciably during the previous 10 hours, when the parcel remains outside the cyclone center in an area of weak sea-surface fluxes. Considering that $\theta_e$is conserved for adiabatic, frictionless motion, one may attribute this abrupt increase in $\theta_e$to the warming associated with diabatic heating.

The energy release shown in Fig. 3 is able to intensify and then to maintain the pressure field in a nearly steady state. To confirm this hypothesis, the θ_e field is analyzed in Fig. 2b for the sensitivity experiment performed by switching off the enthalpy fluxes in the development phase of the cyclone (No-fluxes run). The latter is a restart run starting at 1800 UTC, 6 October 1996 [1]. As mentioned in Yanase et al. (2004), the removal of a certain physical process for a prolonged duration changes not only the vortex itself but

[1] It is obtained by setting the parameters HSFLX and HLFLX = 0 in the subroutine module_sf_myjsfc (sf_sfclay = 2).

For Peer Review

also the environment in which the vortex develops. For this reason, we limit the modification in the physics only to the developing phase of the cyclone, and not to the earlier stages.

Figure 2b shows that the cyclone inner core, although warmer than its surroundings, is cooler by about 10 K compared to the control run. This means that sea surface fluxes have a dramatic impact on the low-level temperature and, as we will show later, on the cyclone intensification. The equivalent of Fig. 3 (not shown) for the No-fluxes experiment shows that the change in θ_e along the parcel trajectory is much smaller than in the control run (about 4 K); thus, without sea surface fluxes, convection is no longer powered by warm and moist air, so that the diabatic heating and the consequent variation in θ_e is limited.

Figure 4 shows the time evolution of the mean sea-level-pressure minimum in the different sensitivity experiments. In the control run, after an initial phase of intensification, the cyclone's pressure minimum remains nearly constant during its transit close to Sardinia, before re-intensifying over the Tyrrhenian Sea. In the No-fluxes run, the cyclone deepens at a similar rate as the control run for the first 12 hours; afterward, the cyclone gets progressively weaker, and the intensification over the Tyrrhenian Sea in the control run is completely missed. Apparently, only in the first few hours of the No-fluxes simulation does the environment remain favorable to the convective heating that can intensify the low pressure.

The different structure of the atmosphere in the two experiments is also illustrated in Fig. 5, where the vertical profiles of θ_e are taken at the same time (1700 UTC, 7 October, corresponding to Fig. 3c for the control run, and 23 h after the restart time in the No-fluxes experiment) at the starting point of the tracks shown in Fig. 2, bringing air parcels toward the center of the cyclone. The warming in the lower levels induced by sea surface fluxes as well as the neutral conditions just above, typical of a tropical cyclone environment, can be identified in the control run (bold line). In contrast, in the No-fluxes run, the low-

For Peer Review

level profile is cooler especially in the lower level, but it still shows a residual instability (thin line). These indications are similar to those emerging in Watanabe and Niino (2014) for a polar mesocyclone over the Japan Sea: in their No-fluxes experiment, cumulus convection could be maintained initially, by collecting the ambient water vapor, but later the absence of surface fluxes resulted in the suppression of cumulus convection. The strong difference between the two profiles in Fig. 5 at around 800 hPa is an indication that the absence of sea-surface fluxes inhibits the triggering of intense convection (as also shown in Fig. 4).

Two additional experiments are shown in Fig. 4, respectively without condensation latent heating (No-latent-heat) and without both surface fluxes and latent heating (No-all). The latter two simulations show a fast weakening of the pressure minimum (after 3 hours, the difference from the control run is 7 hPa), thus diabatic heating is important for the intensification of the cyclone. After about 36 h from the initial time, all three sensitivity experiments show a similar evolution, suggesting that diabatic heating plays a negligible role also in the No-fluxes run after residual instability is removed.

Following Nordeng (1987), if baroclinicity were the most important driving mechanism, one should expect an intensification of the cyclone even in the No-latent-heat (and No-all) run; in contrast, one notes an increase in the pressure minimum after the latent heating (and the surface fluxes) is switched off. Thus, the condensation latent heating appears to be crucial for the development of the TLC in its mature stage, and its contribution to the intensification of the cyclone can be estimated from Fig. 4 at about 10 hPa. However, the fact that, after the initial weakening, the pressure low remains nearly constant in the No-latent-heat (and No-all) run for about 18 hours, indicates that baroclinic instability is still active in preventing the cyclone dissipation.

For Peer Review

In order to analyze the presence of tropical features in the different experiments, we analyzed the evolution of the cyclone in the Hart (2003) diagram parameter space (not shown). In the control run, the cyclone shows a persistent symmetric, warm-core structure during the earlier stage of intensification to the west of Sardinia, and an even warmer upper-level core during its transit over the Tyrrhenian Sea. In the No-fluxes simulation, the warm core is still present during the early stages; later, when the cyclone moves over the Tyrrhenian sea, its characteristics are always those of a cold extra-tropical cyclone. Finally, in the No-latent-heat and in No-all run, the deep warm-core structure is no longer present in the early stage. This is a clear indication of the importance of the WISHE mechanism for the generation of a persistent, symmetric, deep warm core in this case study.

This result is supported by Fig. 6, which shows a vertical cross section near the cyclone center (longitude = 12.45°E) in the control run at 1000 UTC, 9 October 1996, during the transit of the cyclone over the Tyrrhenian Sea (Fig. 6). Features typical of tropical cyclones can be identified (cfr. with Montgomery and Farrell, 1992 and Fig. 9 in Rotunno and Emanuel, 1987), such as ascending motion along absolute momentum $M = u - fy$ (Markowski and Richardson, 2010) (where u is the westerly wind component, f the Coriolis parameter, y the horizontal distance from the center of the cyclone in north-south direction) isosurfaces (lines; zero not shown), large-scale moisture convergence in the low-levels, and a state of nearly-moist neutrality to ascending parcels. Apparently, convection redistributes upward the latent heat acquired near the surface, thus lines of constant θ_e becomes nearly parallel to constant momentum lines. These features do not appear in the sensitivity experiments: the synergic combination of moist convection and sea surface fluxes is thus necessary to provide a cyclone with tropical-like features.

b) *December 2005 case*

For this case study, we started with the model configuration used for the simulation of the first vortex. However, the simulated cyclone made landfall over the northern coast of Libya, far from the observed

For Peer Review

location (see Fig. 2a in Fita and Flounas, 2018). Therefore, we decided to employ the same configuration used in Fita and Flounas (2018), since the latter setup allowed the cyclone to remain over the Mediterranean Sea for a longer time. During the early stages of the cyclone lifetime, the simulated track was similar in the two model configurations, and was very close to the observations, apart from a slight southward shift (cfr. Fig. 7 vs. Fig. 2a in Fita and Flounas, 2018). The crosses of the simulated and the observed cyclone positions are shown in Fig. 7 at 1200 UTC, Dec 14 (red asterisk), and at 1130 UTC, Dec 15 (green "o").

The 900 hPa θ_e and wind vectors are shown in Fig. 8 respectively for the control run and the No-fluxes experiment at 0600 UTC, 14 December, i.e., 18 h after the starting time of the sensitivity experiments (1200 UTC, 13 December), at the time when the cyclone reaches its maximum intensity in the control run (see below). Again, the cyclone inner core in the No-fluxes simulation is colder than in the control run by several K. Compared with the previous case study, the values of low-level θ_e are smaller by about 10 K; however, the SST below the vortex differs only by 1 K between the cyclones and cannot explain for such a large difference. The reasons for that are discussed in the following Section.

The change in $\theta_e$along the back-trajectory for a parcel, representative of the trajectories ending near the center of the cyclone at 900 hPa at 0600 UTC, 14 December, is shown in Fig. 9, together with the snapshots of the 900 hPa θ_e at different times. As for the previous case, a jump in θ_e of about 10 K is simulated when the parcel enters the area affected by intense convection. For the No-fluxes experiment, the change in θ_e is limited to 2 K.

Figure 9a also shows an elongated tongue of warm air extending from the east toward the center of the cyclone just after it has reached the sea surface from the Africa inland. This configuration, which is

For Peer Review

reminiscent of the frontal structure observed in mature extra-tropical cyclones, suggests that baroclinic instability is active in the early stages of cyclone lifetime (which is a typical feature of TLCs, as discussed in Emanuel, 2005).

The evolution of the mean sea-level-pressure minimum in the whole set of sensitivity experiments is shown in Fig. 10 [2]. While in the case of October 1996 the cyclone forms over the sea, and is subject to a strong intensification at the beginning (about 11 hPa in 12 h), the TLC of December 2005 generates inland, deepens strongly as it moves over the sea at around 0200 UTC, 13 December, and intensifies only slightly during the subsequent transit over the Mediterranean Sea (intensification of about 7 hPa in 18 h). In the No-fluxes experiment, the cyclone keeps intensifying for the first 9 h, as in the first case study, but the deepening is limited to about 1 hPa (versus 6 hPa in the same period for the first case); in the No-latent-heat and No-all runs, the pressure minimum remains nearly constant for the first 18 h: this evolution suggests that convection and surface fluxes are important for the intensification of the cyclone. However, the fact that the pressure minimum remains nearly constant in the sensitivity experiments, indicates that a mechanism different from WISHE is acting to prevent the cyclone dissipation. Apparently, baroclinicity has an important effect also on the cyclone evolution, which is confirmed by a diagnostic analysis in terms of Hart (2003) phase space parameters (not shown), where all the sensitivity experiments show a symmetric, warm core for some hours.

Figure 11 shows the vertical profiles of θ_e in the control and No-fluxes run at the same time (0200 UTC, 14 December, corresponding to Fig. 9c in the control run, 14 h after the restart time in the No-fluxes experiment) at the starting points of the tracks shown in Fig. 8, bringing air parcels toward the warmest region in the center of the cyclone at 0600 UTC, 14 December. The vertical profile in the control run is

[2] For the set of parameterization schemes used in this experiment, the surface fluxes are switched off by setting isfflx = 0.

For Peer Review

very close to that of the first case study, being nearly moist neutral above the lower levels, while the low level θ_e is colder by 6K (cf. Fig. 5). The suppression of air-sea interaction processes in the No-fluxes run reduces the temperature in a deeper layer than in the first cyclone, so that the profile above 900 hPa is only slightly unstable. As shown in Fig. 10, compared to the first case study, convection produces only a weak intensification of the cyclone in the No-fluxes run, limited to 1 hPa, possibly due to the smaller extent of the area with high values of θ_e (cf. Fig. 3d with Fig. 9d).

In contrast with the first case, the cyclone never develops a fully tropical-like structure (Fig. 12): the cross section along the cyclone center (latitude = 34.1°E) in the control run at 0600 UTC, 14 December 2005, at the time of maximum intensity, shows that the cyclone is asymmetric, an ascending motion along the absolute momentum $M = v + fx$ (where v is the southerly wind component, x the horizontal distance from the center of the cyclone in east-west direction) isolines directed toward the upper troposphere is in formation and occurs only on the northern side of the cyclone, moisture convergence in the low-levels is weak, high values of θ_e remain confined to the lower levels. In the following section, the motivation for the different behavior of the two cyclones is discussed.

For Peer Review

5. Discussion

Following Markus and Riehl (1960) and Anthes (1982), the surface pressure at any point in a tropical cyclone may be computed hydrostatically from the ascent path of the surface air to the high troposphere. As a consequence, one can estimate the deepening of a tropical cyclone based on the change in θ_e from the external region, where the parcel starts, to the cyclone center, i.e. from the undisturbed region to the area affected by intense air-sea interaction processes: dp = -2.5 dθ_e. Thus, a change in θ_e of around 10 K would cause a surface pressure drop of about 25 hPa; in our cases, one can observe a change of about

386 10-15 hPa in the two cyclones, which can be understood considering that the extent of the troposphere at mid-latitudes (typically up to 300 hPa) is shallower compared to that a typical tropical environment (up to 100 hPa), that convection in the mature stage of Medicanes is often shallow (Miglietta et al., 2013; Dafis et al., 2017) and that the entrainment of dry air can be an important process in the mid-latitudes. Thus, for the Mediterranean, this empirical relationship does not work and its formula should be corrected based on a set of several case studies. This is left for further studies.

Next, we analyze the difference between the two cyclones and the reasons for their different evolution. An investigation of the temperature at 500 and 300 hPa (not shown) indicates that the upper-level environment is similar in the two cases. The comparison of the profiles of θ_e (cf. Fig. 5 with Fig. 11) in the warmest region near the center of the cyclones reinforces the idea of a similar environment, with a moist-neutral profile and similar values of θ_e above the boundary layer. Considering also that the sea-surface temperature differs by only 1 K over the part of the sea surface crossed by the two cyclones (contours in Fig. 13a and Fig. 13c) - the cooler SST in December is partially compensated by the location of the cyclone at more southern latitudes -, one would expect a similar conversion of the heat energy extracted from the ocean into mechanical energy. On the other hand, the low level θ_e changes significantly, with difference of the order of 10 K (cf. Fig. 2 with Fig. 8).

The distribution and intensity of the fluxes in the two cyclones may contribute the explanation of such a large difference[3]. In the first case, the cyclone develops downwind of two dry and cold wind systems: the Tramontane, coming down the Aude valley between the Massif Central and the Pyrenees into the Gulf of Lyon, and the Cierzo, funneled through the Ebro valley (Masson and Bougeault, 1996). (Other channeling winds in Spain also contribute to reinforce the sea-surface fluxes in the western

[3] Other factors, such as the characteristics of the air masses, may be important as well.

For Peer Review

Mediterranean, as shown in Fig. 13a.) These winds are strong and persistent, so that they produce intense sea-surface fluxes in a wide region for a long period, even before the cyclone formation (a similar configuration was observed for an intense cyclone affecting the same area on September 1996; Homar et al., 2003). Thus, the long-lasting and intense transfer of energy from the sea to the atmosphere changes dramatically the values θ_e in the atmospheric boundary layer. The total sea surface fluxes are shown in Fig. 13a at the time of maximum cyclone depth in the early stage of the cyclone lifetime (0300 UTC, October 7). The cyclone develops and persists for several hours (Fig. 1) inside an extensive area characterized by values above 1000 W/m^2, and peaks higher than 1800 W/m^2, values consistent with those expected in tropical storms. Figure 13b shows that the latent-heat fluxes represent the majority of the energy transfer from the surface: contributions from the latent-heat flux outweigh that of the sensible heat flux by a factor of two or three, as generally expected for a Mediterranean TLC (Lagouvardos et al., 1999; Reale and Atlas, 2001).

In contrast, the sea-surface fluxes in the second cyclone are associated more closely with the circulation associated with the vortex. Figure 13c shows their value at the time of maximum intensity (0600 UTC, December 14). The peak is still around 1000 W/m^2, but it is confined in a limited area in the southern part of the cyclone, directly affected by the inflow of dry and cold air from the inland. Again, the latent-heat fluxes represent most of the total sea-surface fluxes (Fig. 13d).

The different sea-surface fluxes have a significant impact on the subsequent evolution of the cyclones. In both cases, the maximum intensity in the early stages is reached when the upper-level PV streamer wraps around the cyclone. This is shown in Figs. 14a and 14c by the low values of potential temperature θ on the isosurface PV = 2 PVU around the cyclone, corresponding to a descent of the dynamic tropopause into mid-troposphere (below 5000 m height in both cases). In the first cyclone, the strong air-sea interaction makes the cyclone able to self-sustain and even to intensify during its following transit

For Peer Review

over the Tyrrhenian Sea: in this phase, an isolated minimum of θ on the 2 PVU surface (i.e., a localized maximum of PV on a constant θ-surface) is diabatically generated by convection (Fig. 14b) and is not connected with any large-scale feature. A similar evolution was observed in idealized numerical experiments using an axisymmetric nonhydrostatic model to reproduce the evolution of a polar low (Emanuel and Rotunno, 1989) and in the simulations of the intense TLC that developed in western Mediterranean on November 2011 (see Figs. 2a, 2b in Miglietta et al., 2017), where a maximum in "wet" PV developed in its mature stage. In contrast, for the second cyclone the weaker sea-surface fluxes do not allow any further development, and the vortex remains connected with the large-scale PV structure in which it formed (Fig. 14d).

For Peer Review

Seen from another perspective, both cyclones develop on the left-hand side of a jet stream, but while in the first case the cyclone progressively moves away from the region of high vertical wind shear, due also to a progressive southward shift of the jet core, in the second case the cyclone remains in the high-shear region associated with the jet stream for all its lifetime. Thus, in the first case the cyclone develops in a barotropic environment, while in the second case the environment remains baroclinic even at later stages of its lifetime.

6. Conclusions

Two Mediterranean tropical-like cyclones are analyzed here by means of high-resolution numerical simulations. For both cases, some recent papers have explained the presence of a symmetric, deep warm core in the cyclone center in terms of baroclinic processes (warm-air seclusion), while their simulations did not provide sufficient evidence that a process similar to WISHE was in place.

Numerical simulations are undertaken here to clarify better the respective role of air-sea interaction and of baroclinic processes in the two cyclones lifetime. Results show the generation of a maximum of θ_e near the cyclones center; in order to investigate the reasons for this warm core, the evolution of θ_e is analyzed for a Lagrangian back-trajectory ending at 900 hPa in a point close to the warmest part of the cyclones. The low-level air parcels move along an inward spiraling convective band, from the outskirts toward the eye, showing an increase in θ_e when the parcels move toward the area affected by the largest sea-surface fluxes and intense convection. In contrast, the $\theta_e$of the parcels does not change appreciably as long as they remain outside the cyclone center. Considering that θ_e is conserved for adiabatic motion, one may attribute the increase in θ_e to warming associated with diabatic heating. Sensitivity experiments, performed without latent-heat release and/or sea-surface fluxes, show that the air-sea interaction and the latent heating due to convection are necessary in order to explain the intensification of both cyclones, suggesting a key role for the WISHE mechanism in the cyclone development. However, the importance of air-sea interaction processes appears to be case dependent.

For the first cyclone, the intense sea-surface fluxes covering a wide region, partially due to the Tramontane and Cierzo wind outbreaks into the Mediterranean Sea, which transfer a large amount of energy from the ocean to the atmosphere in the area where the cyclone developed. As a consequence, the vortex is able to self-sustain even after it moves farther from the upper-level PV streamer in which it developed, to survive in a barotropic environment and to reach a tropical-like structure at a later stage in its lifetime (Fig. 12). Thus, latent-heat release and sea-surface fluxes play a fundamental role for its development, while the role of baroclinicity appears to be minor and confined to the early stages in the cyclone lifetime. Considering that a peak in the genesis and track density of Medicanes occurs around the Balearic Islands (Tous and Romero, 2013; Cavicchia et al., 2014), one may attribute this feature to

For Peer Review

the intense and extensive air-sea interaction processes associated with the strong cold and dry winds frequently occurring in the area.

For the second case, sea-surface fluxes are induced only by the cyclonic circulation around the pressure low and are less intense. In the sensitivity experiments where latent-heat and/or surface fluxes are switched off, the cyclone intensity is still reduced compared to the control run, but remains nearly constant for several hours, suggesting that baroclinic instability prevents the cyclone from dissipating. An analysis in terms of Hart (2003) phase space diagram reveals that a deep warm core may form even excluding sea-surface fluxes and condensational latent heating. Thus, both air-sea interaction and baroclinic processes appear to be active. For this case, the cyclone grows and decays in the baroclinic environment associated with the PV streamer in which it formed, on the left side of a jet stream; the interaction with the PV streamer appears long-lasting and affect its track and intensity also at later stages. The cyclone never develops a fully tropical-like structure, showing only a weak transport of high-$\theta_e$air from the bottom to the top of the troposphere.

This analysis confirms that, even within the category of Mediterranean tropical-like cyclones, different ways of development are possible depending on the large-scale and mesoscale environment in which the cyclones develop. Thus, for Mediterranean TLC one may sustain what Emanuel and Rotunno (1989) noted for polar lows: “there is evidently more than one mechanism operating to produce the spectrum of phenomena called polar lows, although one mechanism may dominate the other in a particular circumstance. One of these mechanisms is certainly baroclinic instability while the other(s) involve … air-sea interaction.” Based on the results of the present paper, we propose a classification of Medicanes in different categories: those dominated in its mature stage by the WISHE mechanism, as the first cyclone (*category A*), and those where both mechanisms appear important even at later stages as the second

For Peer Review

cyclone (*category B*). In both cases, the maximum intensity in the early stages is reached at the time when the upper level PV streamer completely wraps around the cyclone.

The mechanisms of intensification presented here are not exhaustive: for example, the cyclone affecting the Ionian regions on September 2006 (Moscatello et al., 2008b) provides an example of a different way of development, which we propose to classify as *category C*. In that case, a tropical transition and a dramatic intensification occurs after a short but intense interaction of the cyclone with an upper-level PV streamer associated with a different, large-scale cyclone (Figs. 2c and 2d in Miglietta et al., 2017), undergoing a strong intensification as it moved close to the left-exit of a jet stream (Chaboureau et al., 2012).

Additional cases need to be evaluated to provide a comprehensive analysis of the ways different mechanisms can cooperate to determine cyclone evolution. For example, it would be interesting to explore how the different nature of the cyclones discussed here is connected with the location of cyclogenesis, i.e., if western Mediterranean cyclones, which can take advantage of more intense sea fluxes associated with mesoscale winds, can more easily reach a fully tropical-like structure. The analysis presented here and that of the intense cyclone occurring on November 2011 (Miglietta et al., 2017) in the western Mediterranean seem to support this hypothesis.

Finally, sea-surface temperatures are considered as constant and at coarse resolution in the present study. More accurate numerical simulations would require the use of coupled models, where air-sea interaction processes are treated in a consistent way for the atmospheric-, wave- and oceanic-model component, and high-resolution sea temperature can evolve over time. As we have shown, sea-surface fluxes are important for the development of these cyclones and need to be accurately simulated; however, the few studies on the topic have revealed that the corrections in the sea-surface temperature and fluxes, due to

For Peer Review

the use of a coupled numerical system, have only a minor effect both in terms of cyclone intensity and track (see Akhtar et al., 2014; Ricchi et al., 2018).

ACKNOWLEDGEMENTS

MMM gratefully acknowledges the funding from the European Commission (Project "CEASELESS", grant agreement no. 730030). The stays of MMM in Boulder were supported respectively by NCAR and by the CNR Short-Term Mobility Program. Diego Cerrai (University of Connecticut) is gratefully acknowledged for his insightful comments on a first draft of the manuscript.

FIGURE CAPTIONS:

Figure 1: The October 1996 case: simulated track in the control run. The simulated and the observed cyclone positions (eye-based location taken from satellite images) are shown at 1000 UTC, Oct 7 (red asterisk), at 1500 UTC, Oct 8 (green "o"), at 1030 UTC, Oct 9 (blue "x"). The names of the geographic places mentioned in the text are also shown.

Figure 2: The October 1996 case: 900 hPa equivalent potential temperature θ_e and wind vectors at 2100 UTC, 7 October 1996 in the control run (a, top) and in the No-fluxes run (b, bottom). Lagrangian back-trajectories are also shown, ending at 2100 UTC, 7 October in the southern part of the warm core of the cyclone at 900 hPa and starting at 1700 UTC, 7 October.

Figure 3: The October 1996 case: 900 hPa $\theta_e$and 2-hour track in the control run for a parcel whose Lagrangian back-trajectory ends at 2100 UTC, 7 October 1996 in the southern part of the warm core of the cyclone at 900 hPa. θ_e is shown (the track is centered) at 0700 UTC, 7 October (a, top left), 1200 UTC, 7 October (b, top right), 1700 UTC, 7 October (c, bottom left), 2100 UTC, 7 October (d, bottom right). The pressure of the parcel at different times is also shown.

For Peer Review

Figure 4: The October 1996 case: time evolution of the mean sea-level-pressure minimum in the control run and in the sensitivity experiments, No-fluxes, No-latent-heat, and No-all (see text for the description of the different simulations).

Figure 5: The October 1996 case: vertical profiles of θ_e at 1700 UTC, 7 October, at the starting point of the tracks shown in Fig. 2 (bold line for the control run, thin line for the No-fluxes run).

Figure 6: The October 1996 case: vertical cross section of θ_e (colors), storm-relative winds (vectors), absolute momentum (lines, contour interval = 5 m s^{-1}; zero not shown) near the cyclone center (longitude = 12.45°E) in the control run at 1000 UTC, 9 October 1996.

Figure 7: The December 2005 case: simulated track in the control run. The simulated and the observed cyclone positions are shown in Fig. 7 at 1200 UTC, Dec 14 (red asterisk), and at 1130 UTC, Dec 15 (green “o”).

Figure 8: The December 2005 case: 900 hPa equivalent potential temperature θ_e and wind vectors at 0600 UTC, 14 December 2005 in the control run (a, top) and in the No-fluxes run (b, bottom). Lagrangian back-trajectories are also shown, ending at 0600 UTC, 14 December, in the southern part of the warm core of the cyclone at 900 hPa and starting at 0200 UTC, 14 December.

Figure 9: The December 2005 case: 900 hPa $\theta_e$and 2-hour track in the control run for a parcel whose Lagrangian back-trajectory ends at 0600 UTC, 14 December, in the warm core of the cyclone at 900 hPa. θ_e is shown (the track is centered) at 1600 UTC, 13 December (a, top left), 2100 UTC, 13 December (b, top right), 0200 UTC, 14 December (c, bottom left), 0600 UTC, 14 December (d, bottom right). The pressure of the parcel at different times is also shown.

Figure 10: The December 2005 case: time evolution of the mean sea-level-pressure minimum in the control run and in the sensitivity experiments, No-fluxes, No-latent-heat, and No-all.

Figure 11: The December 2005 case: vertical profiles of θ_e at 0200 UTC, 14 December, at the starting point of the tracks shown in Fig. 8 (bold line for the control run, thin line for the No-fluxes run).

For Peer Review

Figure 12: The December 2005 case: vertical cross section of θ_e (colors), storm-relative winds (vectors), absolute momentum (lines, contour interval = 5 m s^{-1}; zero not shown) near the cyclone center (latitude = 34.1°E) in the control run at 0600 UTC, 14 December.

Figure 13: Total (left) and latent-heat (right) sea-surface fluxes (W/m^2; colors), 1000 hPa wind (vectors) and sea-surface temperature (K; contours) at 0300 UTC, October 7 1996 (top), and at 0600 UTC, December 14 (bottom).

Figure 14: θ (K; colors) on the isosurface PV = 2 PVU at 0300 UTC, 7 October 1996 (a, top left), at 1500 UTC, 9 October 1996 (b, top right), at 0600 UTC, 14 December 2005 (c, bottom left), at 0000 UTC, 15 December 2005 (d, bottom right).

For Peer Review

BIBLIOGRAPHY

Akhtar N, Brauch J, Dobler A, Béranger K, Ahrens B. 2014. Medicanes in an ocean—atmosphere coupled regional climate model. *Nat. Hazards Earth Syst. Sci.* **14**: 2189–2201

Anthes RA. 1982. Tropical Cyclones: Their Evolution, Structure and Effects. *Meteorol. Monogr.* **41**. American Meteorological Society, Boston, 298 pp.

Betts AK, Miller MJ. 1993. The Betts-Miller scheme, in *The Representation of Cumulus Convection in Numerical Models*, *Meteorol. Monogr.* **46**: 107–121.

Businger S, Reed RJ. 1989. Cyclogenesis in cold air masses. *Weather and Forecasting* **4**: 133–156.

Cavicchia L, von Storch H, Gualdi S. 2014. A long-term climatology of Medicanes. *Clim. Dyn.* **43**: 1183–1195.

Cavicchia L, Dowdy A, Walsh K. 2018. Energetics and Dynamics of Subtropical Australian East Coast Cyclones: Two Contrasting Cases. *Mon. Weather Rev.* **146**: 1511–1525.

Chaboureau J-P, Pantillon F, Lambert D, Richard E, Claud C. 2012. Tropical transition of a Mediterranean storm by jet crossing, *Q. J. R. Meteorol. Soc.* **138**: 596–611.

602 Cioni G, Cerrai D, Klocke D. 2018. Investigating the predictability of a Mediterranean tropical-like cyclone using a storm-resolving model. *Q. J. R. Meteorol. Soc.* 144, 1598-1610.

604 Dafis S, Rysman J-F, Claud C, Flaounas E. Remote sensing of deep convection within a tropical-like cyclone over the Mediterranean Sea. *Atmos. Sci. Lett.* **19**: e823.

606 Dudhia J. 1989. Numerical study of convection observed during the Winter Monsoon Experiment using a mesoscale two-dimensional model. *J. Atmos. Sci.* **46**: 3077–3107.

608 Dudhia J. 1996. A multi-layer soil temperature model for MM5, Preprints, Sixth PSU/NCAR Mesoscale Model Users Workshop, Boulder, CO, PSU/NCAR, 4950.

610 Emanuel KA. 1986. An air–sea interaction theory for tropical cyclones. Part I: Steady-state maintenance. *J. Atmos. Sci.* **43**: 585–604.

612 Emanuel KA, Rotunno R. 1989. Polar lows as Arctic hurricanes. *Tellus* **41A**: 1–17.

613 Emanuel KA. 2005. Genesis and maintenance of "Mediterranean hurricanes". *Adv. Geosci.* **2**: 217–220.

614 Fita L, Flaounas E. 2018. Medicanes as subtropical cyclones: the December 2005 case from the perspective of surface pressure tendency diagnostics and atmospheric water budget. *Q. J. R. Meteorol. Soc.* **144**: 1028-1044.

617 Gaertner MA, Gonzalez-Aleman JJ, Romera R, Dominguez M, Gil V, Sanchez E, Gallardo C, Miglietta MM, Walsh K, Sein D, Somot S, dell'Aquila A, Teichmann C, Ahrens B, Buonomo E, Colette A, Bastin S, van Meijgaard E, Nikulin G. Simulation of medicanes over the Mediterranean Sea in a regional climate model ensemble: impact of ocean-atmosphere coupling and increased resolution. *Clim. Dyn.* **51**: 1041-1057.

622 Garde LA, Pezza AB, Bye JAT. 2010. Tropical transition of the 2001 Australian duck. *Mon. Weather Rev.* **138**: 2038–2057.

624 González-Alemán JJ, Valero F, Martín-León F, Evans JL. 2015. Classification and synoptic analysis of subtropical cyclones within the northeastern Atlantic Ocean. *J. Clim.* **28**: 3331–3352.

For Peer Review

Hart, RE. 2003. A cyclone phase space derived from thermal wind and thermal asymmetry. *Mon. Weather Rev.* **131**: 585–616.

Homar V, Romero R, Stensrud DJ, Ramis C, Alonso S. 2003. Numerical diagnosis of a small, quasi-tropical cyclone over the western Mediterranean: Dynamical vs. boundary factors. *Q. J. R. Meteorol. Soc.* **129**: 1469–1490.

Hong S-Y, Dudhia J, Chen SH. 2004. A revised approach to ice-microphysical processes for the bulk parameterization of cloud and precipitation. *Mon. Weather Rev.* **132**: 103–120.

Hong S-Y, Noh Y, Dudhia J. 2006. A new vertical diffusion package with an explicit treatment of entrainment processes. *Mon. Weather Rev.* **134**: 2318–2341.

Janjic ZI. 2001. 'Nonsingular implementation of theMellor–Yamada Level 2.5 Scheme in the NCEP Meso model,' NCEP Office Note 437. NCEP: College Park, MD.

Kain JS. 2004. The Kain-Fritsch convective parameterization: An update. *J. Appl. Meteorol.* **43**: 170–181.

Lagouvardos K, Kotroni V, Nickovic S, Jovic D, Kallos G. 1999. Observations and model simulations of a winter sub-synoptic vortex over the central Mediterranean, *Meteorol. Appl.* **6**: 371–383.

Markowski P, Richardson Y. 2010. Mesoscale Meteorology in Midlatitudes. Wiley: New York, NY.

Markus and Riehl (1960)

Masson V, Bougeault P. 1996. Numerical simulation of a low-level wind created by complex orography: A Cierzo case study. *Mon. Weather Rev.* **124**: 701–715.

Mazza E, Ulbrich U, Klein R. 2017. The tropical transition of the October 1996 medicane in the western Mediterranean Sea: A warm seclusion event. *Mon. Weather Rev.* **145**: 2575–2595.

McTaggart-Cowan R, Davies EL, Fairman Jr JG, Galarneau Jr TJ, Schultz, DM. 2015. Revisiting the 26.5°C sea surface temperature threshold for tropical cyclone development. *Bull. Am. Meteorol. Soc.* **96**: 1929–1943.

For Peer Review

Miglietta MM, Moscatello A, Conte D, Mannarini G, Lacorata G, Rotunno R. 2011. Numerical analysis of a Mediterranean hurricane over south-eastern Italy: Sensitivity experiments to sea surface temperature. *Atmos. Res.* **101**: 412–426.

Miglietta MM, Laviola L, Malvaldi A, Conte D, Levizzani V, Price C. 2013. Analysis of tropical-like cyclones over the Mediterranean Sea through a combined modelling and satellite approach. *Geophys. Res. Lett.* **40**: 2400–2405.

Miglietta MM, Mastrangelo D, Conte D. 2015. Influence of physics parameterization schemes on the simulation of a tropical-like cyclone in the Mediterranean sea. *Atmos. Res.* **153**: 360-375.

Miglietta MM, Cerrai D, Laviola S, Cattani E, Levizzani V. 2017. Potential vorticity patterns in Mediterranean ”hurricanes”. *Geophys. Res. Lett.* **44**: 2537–2545.

Mlawer EJ, Taubman SJ, Brown PD, Iacono MJ, Clough SA. 1997. Radiative transfer for inhomogeneous atmosphere: RRTM, a validated correlated k-model for the longwave. *J. Geophys. Res.* **102**: 16663–16682.

Montgomery MT, Farrell, BF. 1992. Polar low dynamics. *J. Atmos. Sci.* **49**: 2484-2505.

Moscatello A, Miglietta MM, Rotunno R. 2008a. Observational analysis of a Mediterranean ‘hurricane’ over south-eastern Italy. *Weather* **63**: 306–311.

Moscatello A, Miglietta MM, Rotunno R. 2008b. Numerical analysis of a Mediterranean “hurricane” over southeastern Italy, *Mon. Weather Rev.* **136**: 4373–4397.

Niu G-Y, Yang Z-L, Mitchell KE, Chen F, Ek MB, Barlage M, Longuevergne L, Kumar A, Manning K, Niyogi D, Rosero E, Tewari M, Xia Y. 2011. The community Noah land surface model with multiparameterization options (Noah-MP): 1. Model description and evaluation with local scale measurements. *J. Geophys. Res.* **116**: D12109.

Nordeng, TE. 1987. The effect of vertical and slantwise convection on the simulation of polar lows. *Tellus* **39A**: 354–376.

For Peer Review

Nordeng, TE. 1990. A model-based diagnostic study of the development and maintenance mechanism of trwo polar lows. *Tellus* **42A**: 92–108.

Palmén E. 1948. On the formation and structure of tropical hurricanes. *Geophysica* **3**: 26–38.

Rasmussen E., Zick C. 1987. A subsynoptic vortex over the Mediterranean with some resemblance to polar lows. *Tellus* **39A**: 408-425.

Reale O, Atlas R. 2001. Tropical cyclone-like vortices in the extratropics: Observational evidence and synoptic analysis. *Weather and Forecasting* **16**: 7–34.

Ricchi A, Miglietta MM, Barbariol F, Benetazzo A, Bergamasco A, Bonaldo D, Cassardo C, Falcieri FM, Modugno G, Russo A, Sclavo M, Carniel S. Sensitivity of a Mediterranean tropical-like cyclone to different model configurations and coupling strategies. *Atmosphere* **2017**: *8*, 92, 1-32.

Rotunno R, Emanuel K. 1987. An air–sea interaction theory for tropical cyclones. Part II: Evolutionary study using a nonhydrostatic axisymmetric numerical model. *J. Atmos. Sci.* **44**: 542–561.

Skamarock WC, Klemp JB, Dudhia J, Gill DO, Barker DM, Duda M, Huang X-Y, Wang W, Powers JG. 2008. 'A description of the advanced research WRF Version 3'. NCAR Technical Note NCAR/TN–475+STR. NCAR: Boulder, CO.

Thompson G, Field PR, Rasmussen RM, Hall WD. 2008. Explicit forecasts of winter precipitation using an improved bulk microphysics scheme. Part II: Implementation of a new snow parameterization. *Mon. Weather Rev.* **136**: 5095–5115.

Tous M, Romero R. 2013. Meteorological environments associated with Medicane development, *Int. J. Climatol.* **33**: 1–14.

Yanase W, Fu G, Niino H, Kato T. 2004. A polar low over the Japan Sea on 21 January 1997. Part II: A numerical study. *Mon. Weather Rev.* **132**: 1552–1574,

Yanase W, Niino H. 2018. Environmental control of tropical, subtropical, and extratropical cyclone development over the North Atlantic Ocean: Idealized numerical experiments. *Q. J. R. Meteorol. Soc.* **144**: 539–552.

For Peer Review

Watanabe SI, Niino H. 2014: Genesis and development mechanisms of a polar mesocyclone over the Japan Sea. *Mon. Weather Rev.* **142**: 2248–2270.

For Peer Review

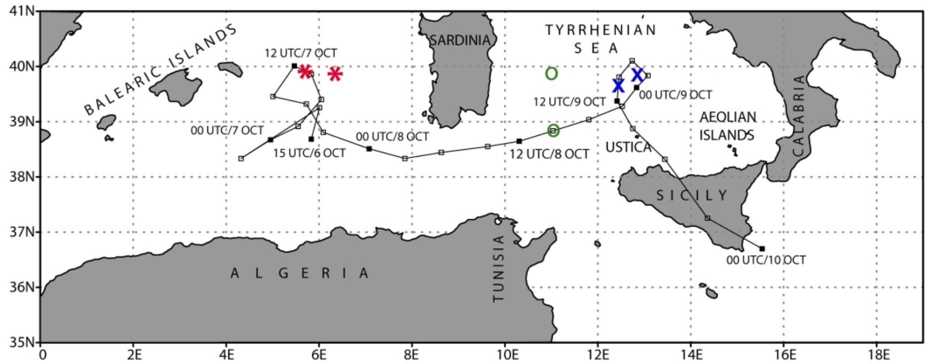

Figure 1: The October 1996 case: simulated track in the control run. The simulated and the observed cyclone positions (eye-based location taken from satellite images) are shown at 1000 UTC, Oct 7 (red asterisk), at 1500 UTC, Oct 8 (green "o"), at 1030 UTC, Oct 9 (blue "x"). The names of the geographic places mentioned in the text are also shown.

279x215mm (300 x 300 DPI)

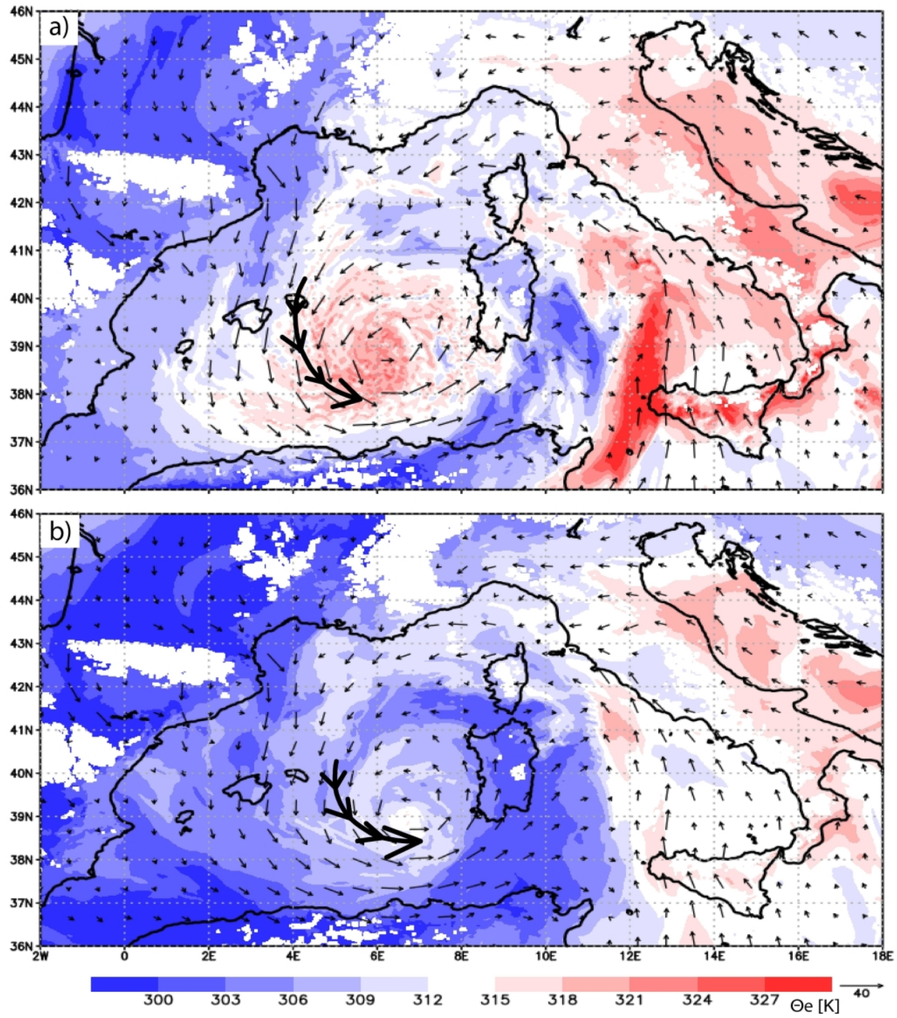

Figure 2: The October 1996 case: 900 hPa equivalent potential temperature θ_e and wind vectors at 2100 UTC, 7 October 1996 in the control run (a, top) and in the No-fluxes run (b, bottom). Lagrangian back-trajectories are also shown, ending at 2100 UTC, 7 October in the southern part of the warm core of the cyclone at 900 hPa and starting at 1700 UTC, 7 October.

215x279mm (300 x 300 DPI)

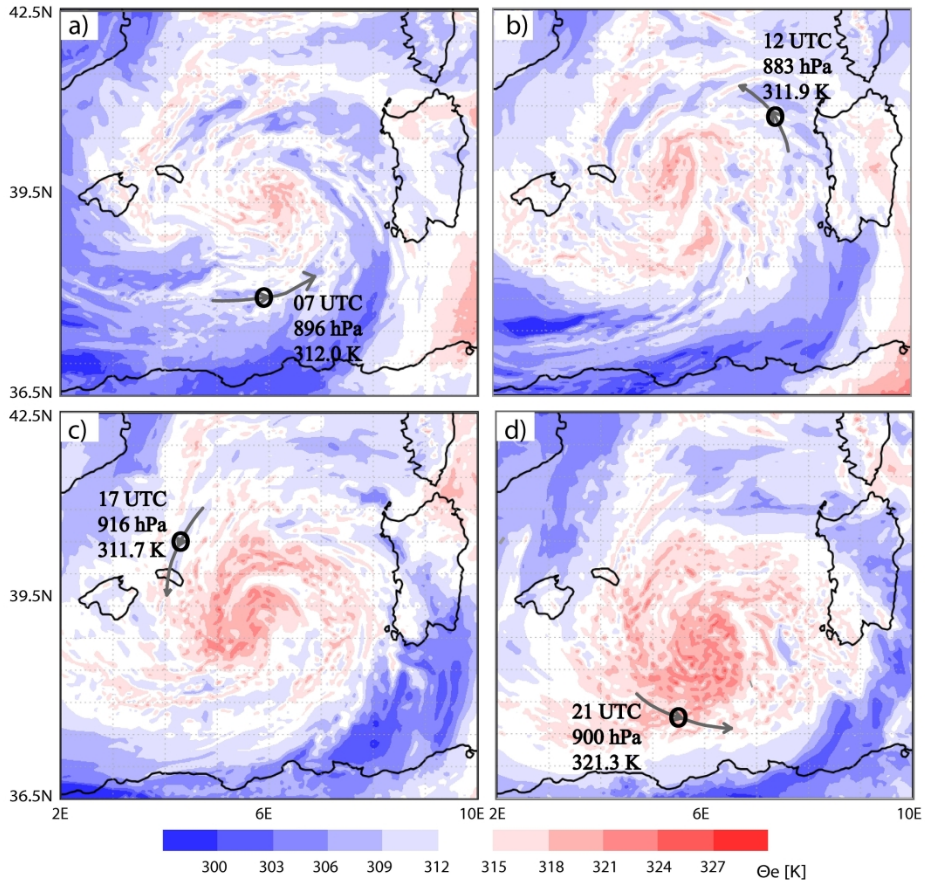

Figure 3: The October 1996 case: 900 hPa θ_e and 2-hour track in the control run for a parcel whose Lagrangian back-trajectory ends at 2100 UTC, 7 October 1996 in the southern part of the warm core of the cyclone at 900 hPa. θ_e is shown (the track is centered) at 0700 UTC, 7 October (a, top left), 1200 UTC, 7 October (b, top right), 1700 UTC, 7 October (c, bottom left), 2100 UTC, 7 October (d, bottom right). The pressure of the parcel at different times is also shown.

215x279mm (300 x 300 DPI)

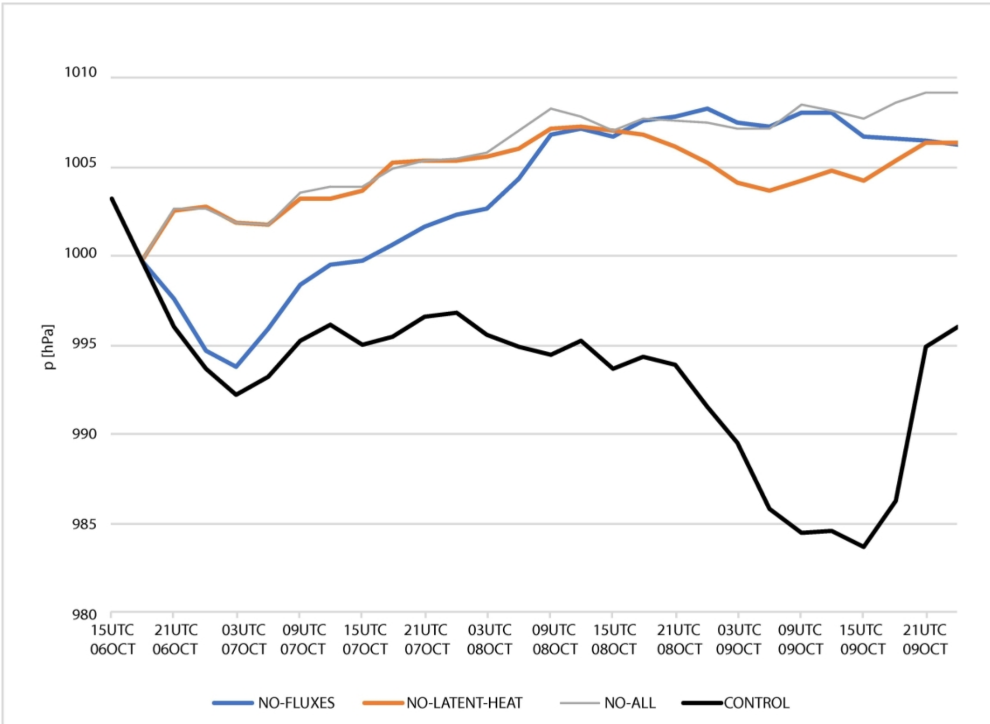

Figure 4: The October 1996 case: time evolution of the mean sea-level-pressure minimum in the control run and in the sensitivity experiments, No-fluxes, No-latent-heat, and No-all (see text for the description of the different simulations).

176x128mm (300 x 300 DPI)

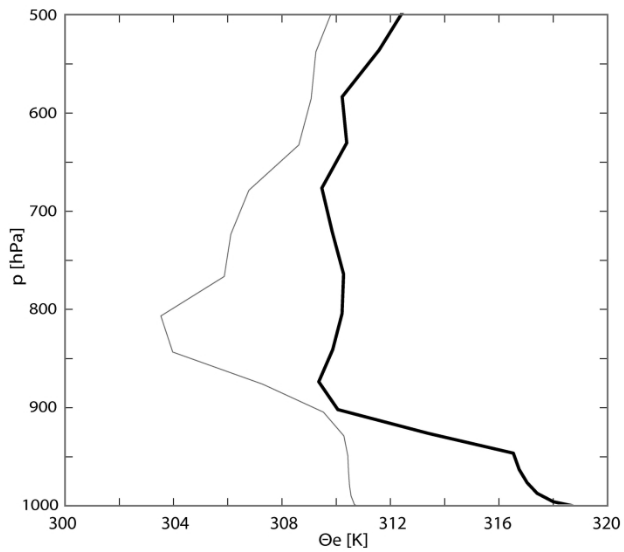

Figure 5: The October 1996 case: vertical profiles of θe at 1700 UTC, 7 October, at the starting point of the tracks shown in Fig. 2 (bold line for the control run, thin line for the No-fluxes run).

215x279mm (300 x 300 DPI)

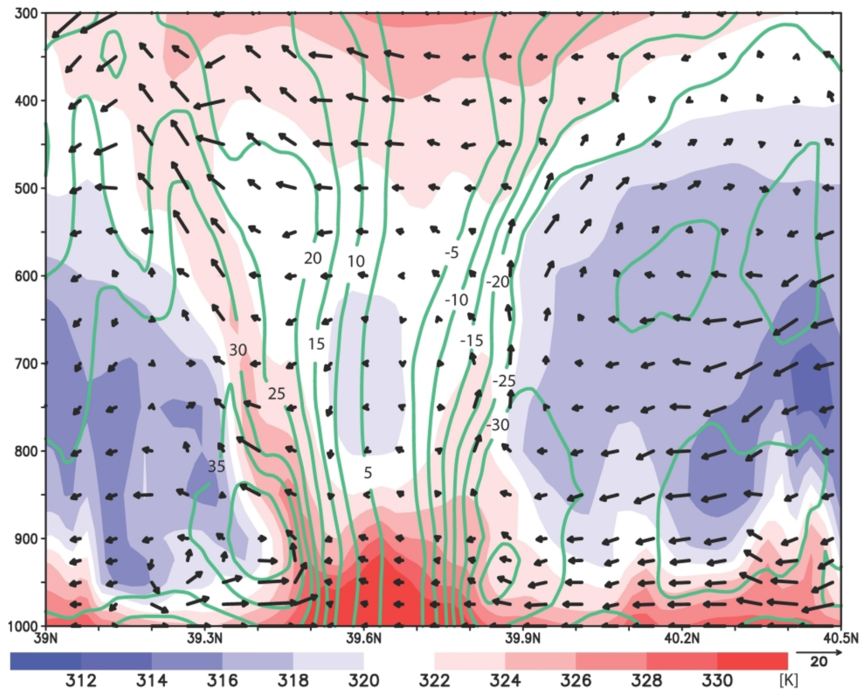

Figure 6: The October 1996 case: vertical cross section of θ_e (colors), storm-relative winds (vectors), absolute momentum (lines, contour interval = 5 m s-1; zero not shown) near the cyclone center (longitude = 12.45°E) in the control run at 1000 UTC, 9 October 1996.

279x215mm (300 x 300 DPI)

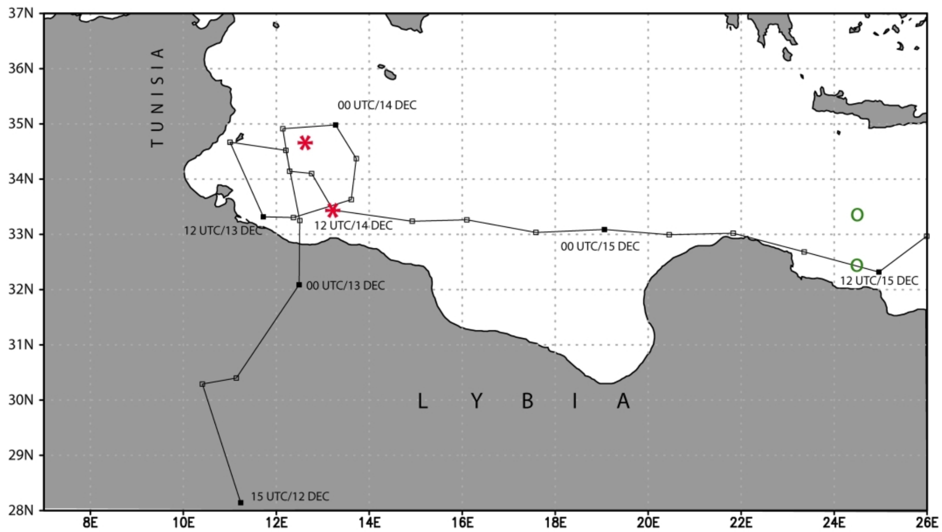

Figure 7: The December 2005 case: simulated track in the control run. The simulated and the observed cyclone positions are shown in Fig. 7 at 1200 UTC, Dec 14 (red asterisk), and at 1130 UTC, Dec 15 (green "o").

279x215mm (300 x 300 DPI)

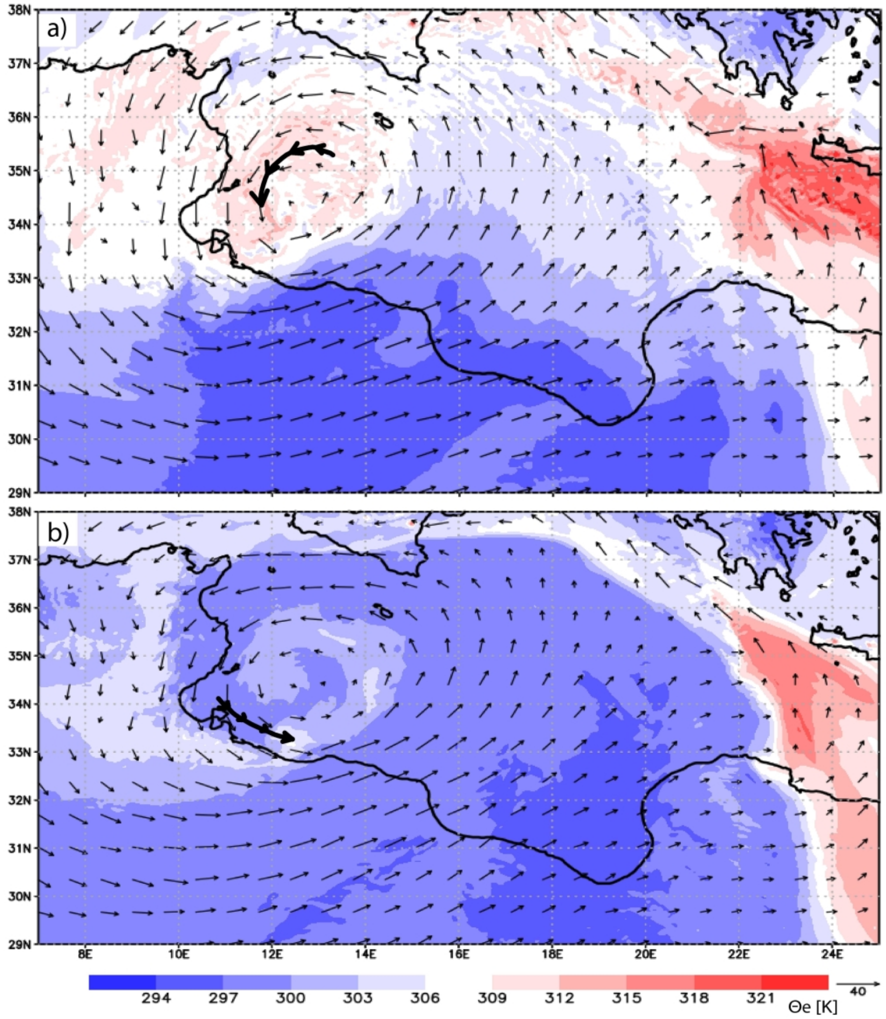

Figure 8: The December 2005 case: 900 hPa equivalent potential temperature θ_e and wind vectors at 0600 UTC, 14 December 2005 in the control run (a, top) and in the No-fluxes run (b, bottom). Lagrangian back-trajectories are also shown, ending at 0600 UTC, 14 December, in the southern part of the warm core of the cyclone at 900 hPa and starting at 0200 UTC, 14 December.

215x279mm (300 x 300 DPI)

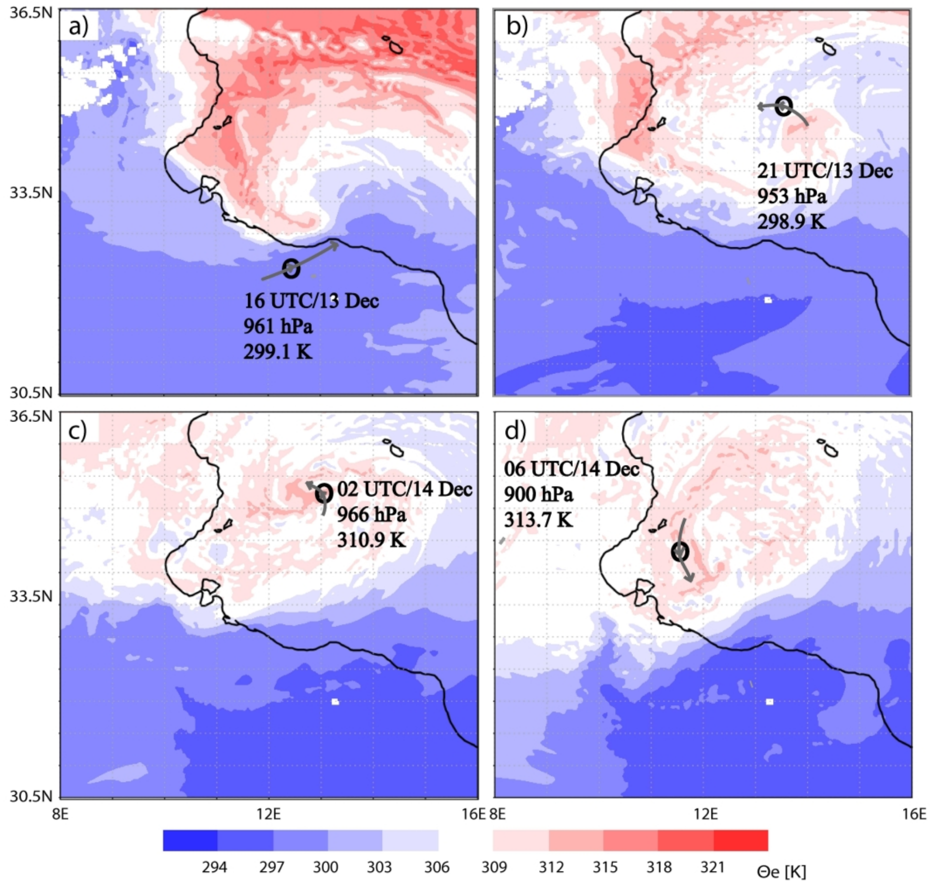

Figure 9: The December 2005 case: 900 hPa θ_eand 2-hour track in the control run for a parcel whose Lagrangian back-trajectory ends at 0600 UTC, 14 December, in the warm core of the cyclone at 900 hPa. θ_e is shown (the track is centered) at 1600 UTC, 13 December (a, top left), 2100 UTC, 13 December (b, top right), 0200 UTC, 14 December (c, bottom left), 0600 UTC, 14 December (d, bottom right). The pressure of the parcel at different times is also shown.

215x279mm (300 x 300 DPI)

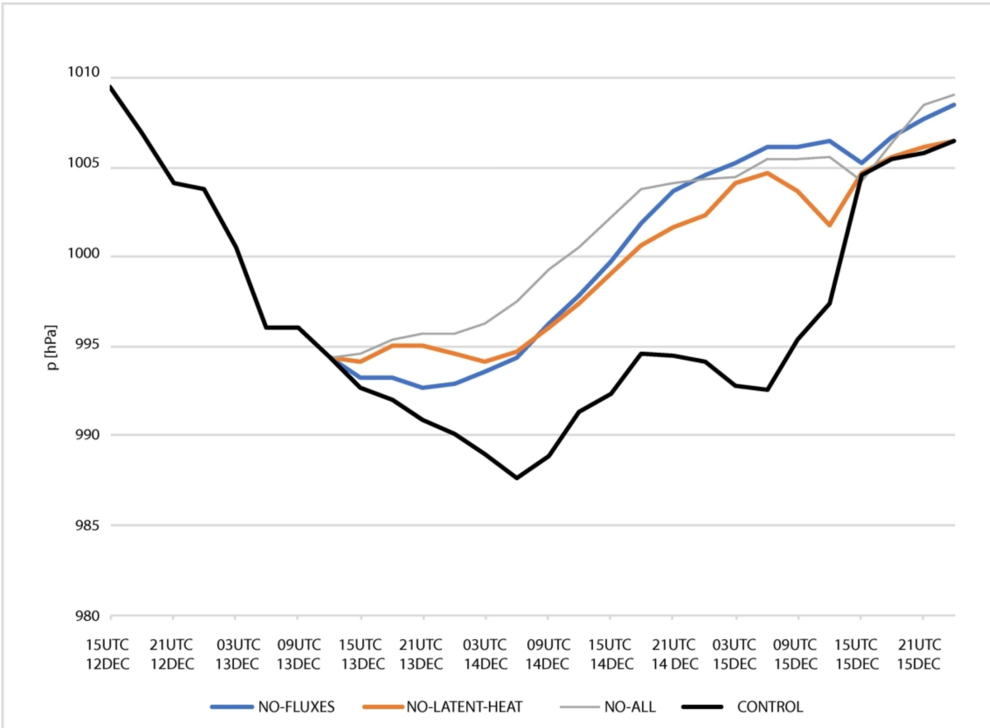

Figure 10: The December 2005 case: time evolution of the mean sea-level-pressure minimum in the control run and in the sensitivity experiments, No-fluxes, No-latent-heat, and No-all.

176x129mm (300 x 300 DPI)

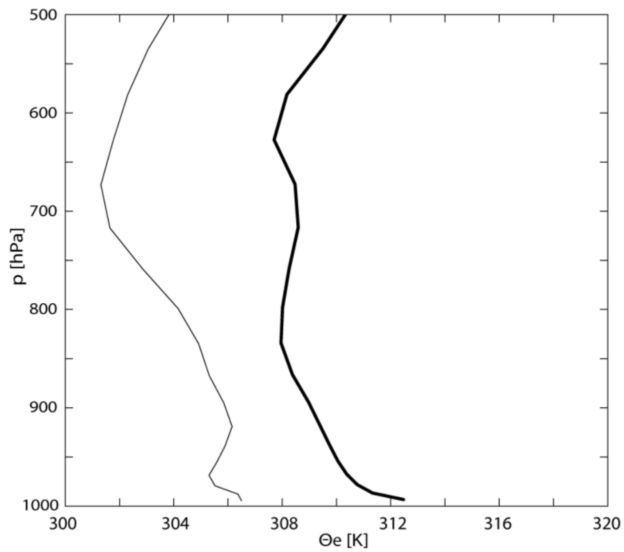

Figure 11: The December 2005 case: vertical profiles of θ_e at 0200 UTC, 14 December, at the starting point of the tracks shown in Fig. 8 (bold line for the control run, thin line for the No-fluxes run).

215x279mm (300 x 300 DPI)

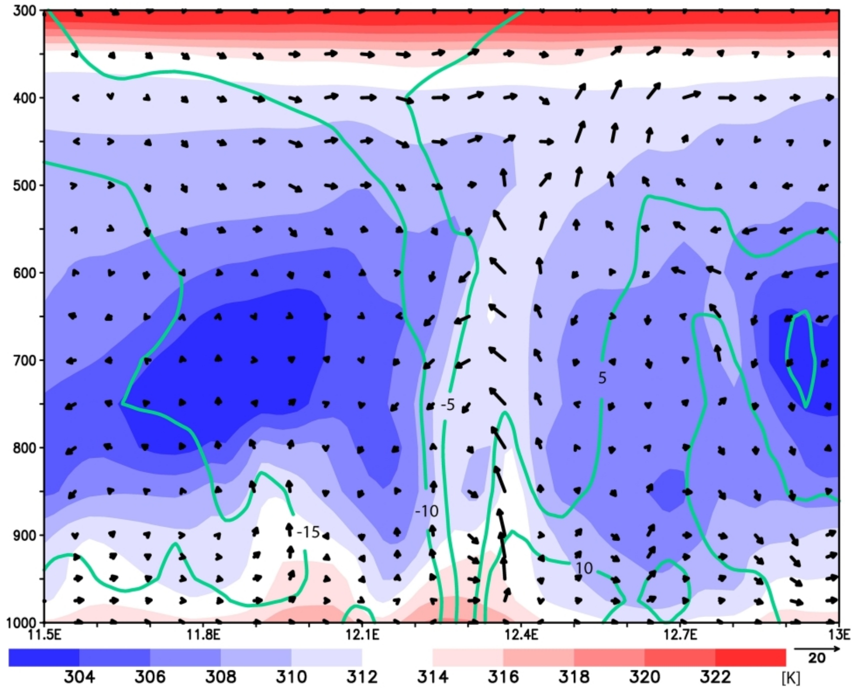

Figure 12: The December 2005 case: vertical cross section of θ_e (colors), storm-relative winds (vectors), absolute momentum (lines, contour interval = 5 m s-1; zero not shown) near the cyclone center (latitude = 34.1°E) in the control run at 0600 UTC, 14 December.

279x215mm (300 x 300 DPI)

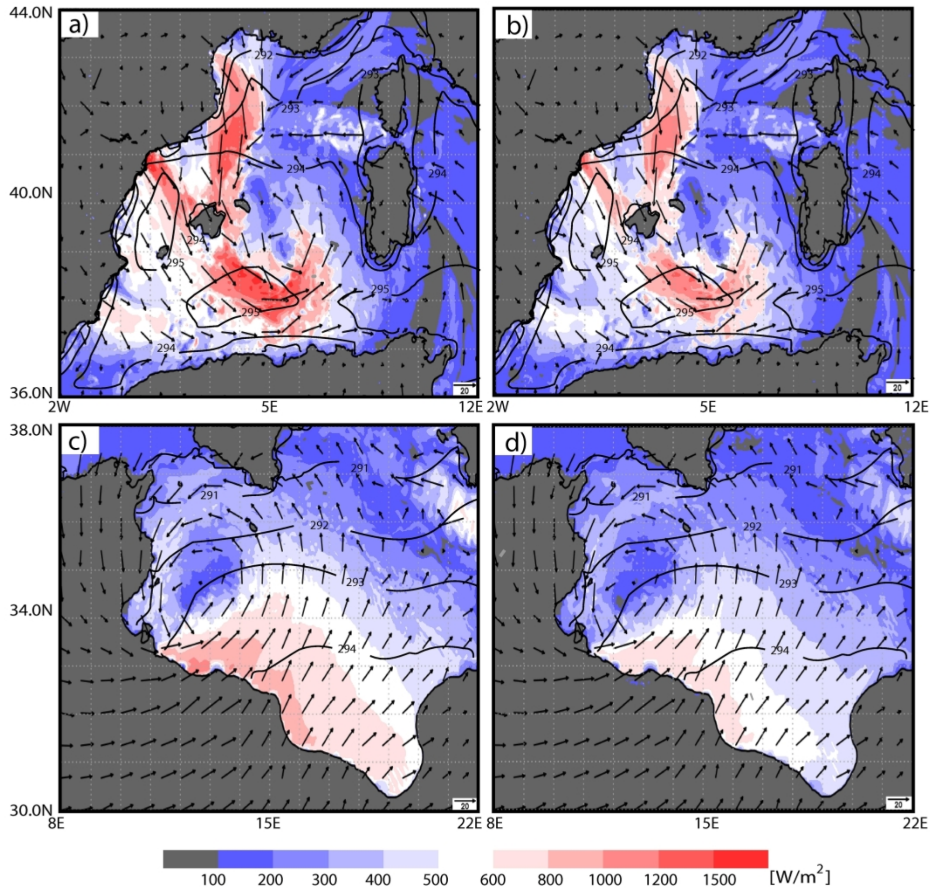

Figure 13: Total (left) and latent-heat (right) sea-surface fluxes (W/m2; colors), 1000 hPa wind (vectors) and sea-surface temperature (K; contours) at 0300 UTC, October 7 1996 (top), and at 0600 UTC, December 14 (bottom).

215x279mm (300 x 300 DPI)

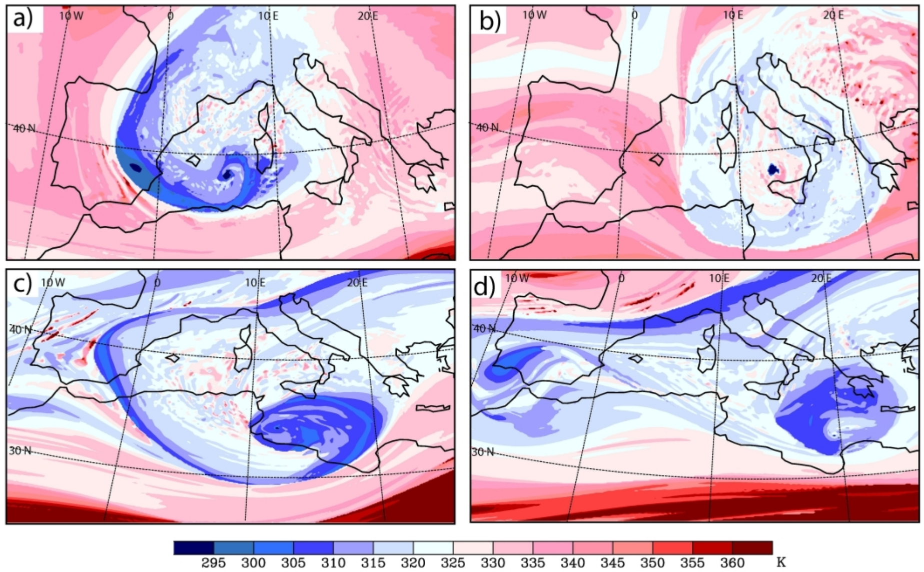

Figure 14: θ (K; colors) on the isosurface PV = 2 PVU at 0300 UTC, 7 October 1996 (a, top left), at 1500 UTC, 9 October 1996 (b, top right), at 0600 UTC, 14 December 2005 (c, bottom left), at 0000 UTC, 15 December 2005 (d, bottom right).

215x279mm (300 x 300 DPI)